# Molecular Origin of the Self-Assembly of Lanreotide into Nanotubes: A Mutational Approach

Céline Valéry,* Emilie Pouget,[†] Anjali Pandit,[‡] Jean-Marc Verbavatz,[‡] Luc Bordes,[‡] Isabelle Boisdé,[‡] Roland Cherif-Cheikh,* Franck Artzner,[†] and Maité Paternostre[‡]

*Ipsen Pharma, 08980 Sant Feliu de Llobregat, Barcelona, Spain; [†]Unité mixte de Recherche du Centre National pour la Recherche Scientifique 6626, Université Rennes 1, F-35042 Rennes, France; and [‡]Institut de Bio Technologies de Saclay, Commisariat à l'Energie Atomique et Centre National pour la Recherche Scientifique, F-91191 Gif-sur-Yvette, France

ABSTRACT Lanreotide, a synthetic, therapeutic octapeptide analog of somatostatin, self-assembles in water into perfectly hollow and monodisperse (24-nm wide) nanotubes. Lanreotide is a cyclic octapeptide that contains three aromatic residues. The molecular packing of the peptide in the walls of a nanotube has recently been characterized, indicating four hierarchical levels of organization. This is a fascinating example of spontaneous self-organization, very similar to the formation of the gas vesicle walls of *Halobacterium halobium*. However, this unique peptide self-assembly raises important questions about its molecular origin. We adopted a directed mutation approach to determine the molecular parameters driving the formation of such a remarkable peptide architecture. We have modified the conformation by opening the cycle and by changing the conformation of a Lys residue, and we have also mutated the aromatic side chains of the peptide. We show that three parameters are essential for the formation of lanreotide nanotubes: i), the specificity of two of the three aromatic side chains, ii), the spatial arrangement of the hydrophilic and hydrophobic residues, and iii), the aromatic side chain in the β-turn of the molecule. When these molecular characteristics are modified, either the peptides lose their self-assembling capability or they form less-ordered architectures, such as amyloid fibers and curved lamellae. Thus we have determined key elements of the molecular origins of lanreotide nanotube formation.

## INTRODUCTION

Self-assembly is characterized by spontaneous diffusion and specific association of molecules dictated by noncovalent interactions. It can be biologically inspired given that the cells contain numerous functional nanostructures built from molecular self-assembly, such as membranes, actin filaments, tubules, chromosomes, flagella, and cytoskeleton. But self-association processes are also essential during biological processes such as protein folding, molecular recognition, and enzyme-substrate binding.

The key elements of molecular self-assembly are a complementary shape between the individual components and weak noncovalent interactions. For biological materials, these noncovalent interactions are typically hydrogen bonds (intra- and intermolecular and with water), ionic bonds, hydrophobic effects, and electrostatic and van der Waals interactions. Although many of these interactions are weak (<5 kcal/mol), their large numbers make the final architectures highly stable. Another consequence of these types of interactions is the possibility of rapid exchange between a molecule involved in the architecture and an external molecule in solution. This implies that the self-assemblies have dynamic properties and a kind of ''self-repair'' faculty. Therefore, central to mimicking biologically inspired self-assembly is the understanding of the forces that govern the thermodynamic stability and

specificity of naturally occurring self-assembly. The emergence of amyloid-related diseases has further increased scientific interest in this field (1–4). Moreover, the possibility of creating nanomaterials of controlled size by using biomimetic molecules has extended the appeal to other scientific fields, especially physics and chemistry (5–9).

In this respect, synthetic small molecules like peptides and/ or lipids with self-assembling properties are explored extensively because of their simplicity, which offers the prospect of understanding the molecular mechanisms driving the self-assembly processes. The bioinspired strategy for the design of simple self-assembling peptides is mainly applied in the de novo synthesis of peptides. For example, Ghadiri's group has explored the self-assembling properties of cyclic synthetic peptides forming nanotubes of molecular dimensions through molecular stacking mediated by unidirectional hydrogen bonds (10–12). A second hierarchical level of organization can be induced by generating self-assemblies between the one-dimensional nanotubes, leading finally to bundles of nanotubes. Another remarkable example is the polar lipid mimicking peptides designed by Zhang et al. (13). These lipid-like peptides self-assemble into architectures usually adopted by polar lipids like nanotubes and/or vesicular structures, underlining the importance of amphiphilicity in molecular packing.

Because of the emergence of prion-related diseases, people are also working extensively on the molecular processes that drive the formation of a special type of architecture formed by the self-assembly of misfolded proteins, generally called ''amyloid'' fibers. The term ''amyloid'', meaning ''starch-like'', was originally applied by mistake to extracellular

protein aggregates found in the organs of patients suffering from amylose, because these aggregates were stained by iodine as is starch (14). Later, it was discovered that amyloids were in fact protein precipitates constituted by ordered fiber/filament structures, which were stabilized by extended intermolecular $\beta$-sheet (15). In this article we apply the term ''amyloid'' to fibers, filaments, and even nanotubes structures when they are proved to be stabilized by an intermolecular $\beta$-sheet network.

Not only prion proteins but also various natural peptides and proteins have been shown to self-assemble in vitro into amyloid-like $\beta$-sheet-rich supramolecular fibrils (4,16–18), leading to the idea that the amyloid state is a common feature of proteins (20). In addition, recent studies point out the involvement of such self-assembled amyloid fibrils in the formation of biofilm and aerial hyphae by microorganisms (21–23), underlining the importance of these particular supramolecular architectures. Whatever the protein studied, the inner supramolecular structure of amyloids relies on intermolecular $\beta$-sheet hydrogen-bond networks along the fibril director, the so-called ''cross-$\beta$'' organization (24). At the

molecular level, $\pi-\pi$ interactions have been proposed to play a significant role in the nucleation process (25) and in the cohesion of characteristic amyloid fibers (26,27).

The major difficulty in understanding the precise molecular organization of amyloid fibers stems from the common feature shared by these supramolecular architectures: they are not three-dimensional crystals but rather disordered precipitates/aggregates of intrinsically ordered fibers. This disorder generates difficulties in establishing the detailed molecular organization. To overcome this problem and to gain detailed information on the molecular interactions involved in the mechanisms of formation of prion amyloid fibers, numerous studies have been performed on peptides extracted from the sequence of native prion proteins that retain self-assembly properties (28–32). Even crystals of amyloid fibers have recently been obtained, allowing the resolution of the precise molecular organization of the amyloid peptide studied (3).

Valéry et al. (33,34) have recently shown that the cyclic octapeptide lanreotide self-associates into nanotubes in the presence of water. Lanreotide (Fig. 1 $a$; DNal-Cys-Tyr-DTrp-Lys-Val-Cys-Thr-CONH$_2$) is a synthetic therapeutic
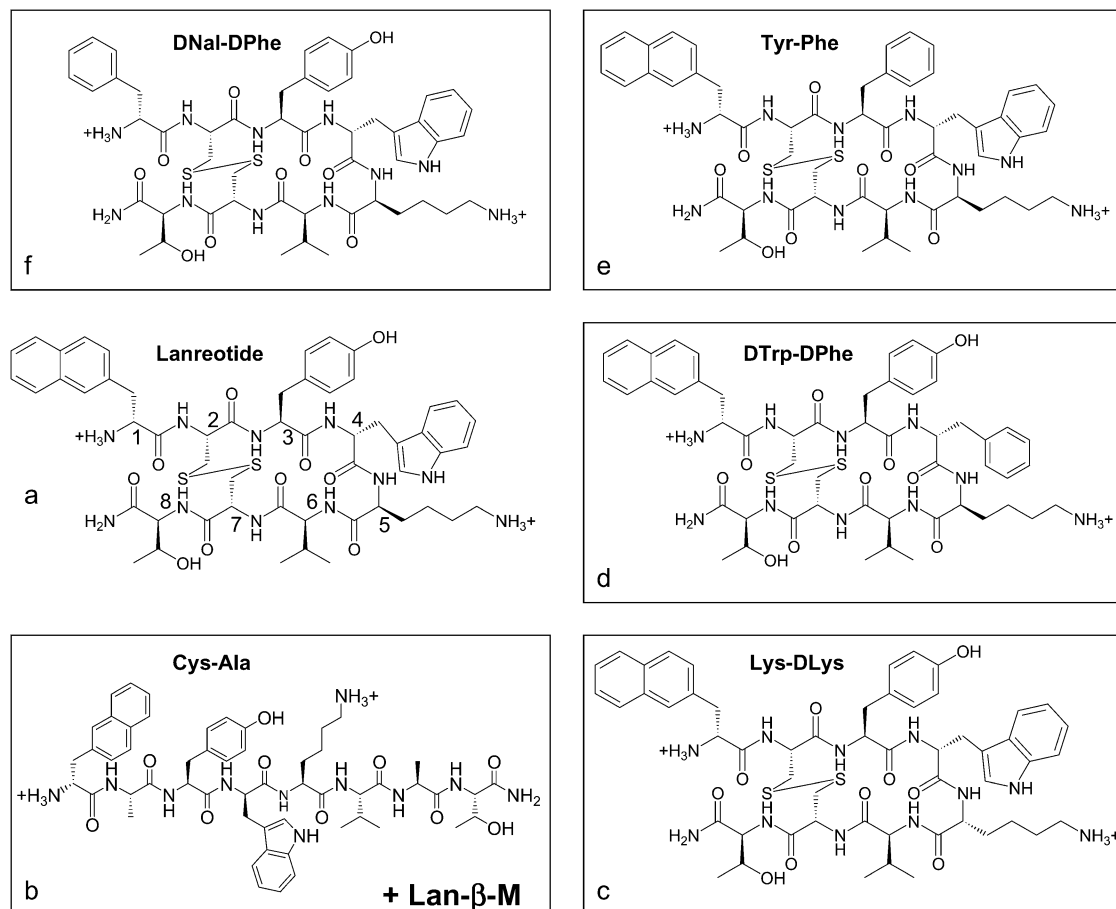


FIGURE 1   Chemical structure of lanreotide ($a$) and its derivatives named Cys-Ala and Lan-$\beta$-M ($b$), Lys-DLys ($c$), DTrp-DPhe ($d$), Tyr-Phe ($e$), and DNal-DPhe ($f$). The numbers 1–8 on the peptide backbone of lanreotide indicate the positions of the amino acids. All the peptides contain 2 mol of acetate per mole of peptide, the acetate being the counterion of the two positive charges of the peptides.

peptide used mainly in the treatment of acromegaly (35). The most remarkable features of these nanotubes are their monodisperse diameter (24 nm) and their relatively large size when compared to the size of the peptide. Thanks to this exceptional monodispersity, the peptide packing in these self-assemblies has been determined (34). This packing exhibits as many as four hierarchical levels of organization, which are, from the lowest to the highest, 1), dimers of peptides essentially stabilized by hydrophobic effects and aromatic side-chain interaction; 2), amyloid filaments generated by the packing of peptide dimers through an intermolecular antiparallel β-sheet network between the peptide backbones, i.e., a typical ''cross-β'' organization; 3), nanotubes generated by the lateral packing of 26 filaments, in which the H-bond network lies flat on the nanotube surface; and 4), the packing of the nanotubes in a hexagonal lattice. The temperature/concentration phase diagram of lanreotide has also been determined and indicates that the nanotubes are at thermodynamic equilibrium and reversible (33).

Such a detailed description of the molecular and supramolecular organization is unique in the field of synthetic biomimetic assembly. This hierarchical peptide organization, completely new and not previously described for peptide self-assemblies, is very similar to the organization of the hydrophobic proteins forming the wall of the gas vesicles of *Halobacterium halobium* (36,37). Indeed, both the lanreotide nanotubes and the gas vesicles walls are bilayers formed by the lateral assembly of fibers formed by two protofilaments. Moreover, as for lanreotide, the peptide skeleton and therefore the H-bond networks lie flat on the surfaces of the walls. However, this type of organization is very rare even in nature. In general, self-assemblies such as amyloid-type fibers present only two hierarchical levels of organization, i.e., the one-dimensional packing of the protein/peptide mediated by intermolecular β-sheet, leading to twisted fibrils, and the fibril assembly into the final fibers, called lamination by Aggeli et al. (38). For this type of aggregate, it is also possible to see a few examples of hollow tubular morphology of amyloid fibers (32,39,40). Nevertheless, the exceptionally ordered lanreotide self-assembly immediately raises the question of the molecular parameters driving this organization.

In this work, we have adopted a mutational approach to test the role of different molecular parameters in the organization of self-assembly structures such as the β-hairpin conformation and the aromatic residue.

Lanreotide adopts a β-hairpin conformation in organic solvents (41,42), a conformation that is stabilized for the peptide self-assembled in nanotubes (33,34). There are at least two molecular parameters stabilizing this conformation: i), the succession of D and L amino acids at positions 4 and 5, i.e., D-Trp followed by L-Lys, inducing a turn in the peptide backbone; and ii), the presence of the two cysteines that form a disulfide bridge in a *gauche-gauche-gauche* (*g-g-g*) conformation (Fig. 1 *a*). To test the role of the molecular conformation in lanreotide packing, we studied three derivatives,

i.e., Lys-DLys in which the conformation of the lysine residue has been modified, the Cys-Ala in which the two Cys have been replaced by two Ala, and the Lan-β-M obtained by treatment of lanreotide with β-mercaptoethanol to obtain two free sulfhydryl (SH) groups instead of the initial disulfide bond (Fig. 1, *b* and *c*).

Lanreotide also possesses three aromatic residues (D-naphthylalanine, tyrosine, and D-tryptophan) that are all segregated on one branch of the β-hairpin (Fig. 1 *a*). In our previous work we showed that this aromatic-aliphatic segregation is enhanced in the supramolecular architectures at each of the four hierarchical levels of organization, thus demonstrating the involvement of the aromatic residues in lanreotide self-assembly. In this work, we mutated each of these aromatic side chains into another aromatic residue, i.e., Phe, to test the specificity of the aromatic side chains of lanreotide. Three derivatives are tested here in which we successively substituted the DTrp, the LTyr, and the DNal aromatic groups by Phe in accordance with the conformation in the lanreotide molecule.

The study was performed using infrared and Raman spectroscopies to determine the conformations of the molecules, small angle x-ray scattering (SAXS) and wide angle x-ray scattering (WAXS) to obtain structural information on the self-assemblies, and optical and electron microscopy to characterize the morphology of the structures formed.

## MATERIALS AND METHODS

### Materials

In Fig. 1, the lanreotide molecule has been drawn together with the derivatives synthesized for this study. Lanreotide ($NH_3^+$-DNal-Cys-Tyr-DTrp-Lys-Val-Cys-Thr-$CONH_2$) and its derivatives were obtained from Ipsen-Pharma (Barcelona, Spain) as acetate salts. The names and formulae of the derivatives are Cys-Ala ($NH_3^+$-DNal-*Ala*-Tyr-DTrp-Lys-Val-*Ala*-Thr-$CONH_2$), Lys-DLys ($NH_3^+$-DNal-Cys-Tyr-DTrp-*DLys*-Val-Cys-Thr-$CONH_2$), DTrp-DPhe ($NH_3^+$-DNal-Cys-Tyr-*DPhe*-Lys-Val-Cys-Thr-$CONH_2$), Tyr-Phe ($NH_3^+$-DNal-Cys-*Phe*-DTrp-Lys-Val-Cys-Thr-$CONH_2$), and DNal-DPhe ($NH_3^+$-*DPhe*-Cys-Tyr-DTrp-Lys-Val-Cys-Thr-$CONH_2$). The peptides were synthesized by a Kinerton batch process (Dublin, Ireland), which includes a flash-freeze lyophilization. Also, 99.9% glycerol, 99% solid naphthalene, and 14 M β-mercaptoethanol were from Sigma (Paris, France).

### Sample preparation

Lanreotide acetate aqueous solutions up to 10% w/w and all the solutions of derivative peptides were prepared by adding deionized water to a weighted fraction of lanreotide acetate powder. For peptide concentrations higher than 10% w/w, the viscosity of the mixtures required the application of a special mixing technique. The system used consisted of two plastic syringes of 2 ml connected by a small tap. One syringe was filled with a weighted fraction of peptide powder, and the other was filled with a weighted fraction of water. The syringe containing the peptide was connected to the tap and a vacuum was produced with a water pump. The other syringe was then connected to the tap and the mixture realized by passing the dispersion from one syringe to the other until total homogenization. The samples were generally prepared 24 h before the experiments and stored at 4°C. For the Lys-DLys derivative, the samples were examined at different times after preparation.

## Optical microscopy

Optical microscopy experiments were realized at room temperature ($\sim$20°C) with crossed polarizers (or phase contrast) using a type 120 Nikon microscope equipped with a Nikon 20 objective (Nikon, Tokyo, Japan). The photographs were obtained with a Nikon Coolpix 950 digital camera. The samples observed were conditioned either in 1.3 mm glass capillaries or between glass slices.

## Small angle x-ray scattering

X-ray patterns were collected with a Mar345 Image-Plate detector (Maresearch, Norderstedt, Germany) mounted on a rotating anode x-ray generator FR591 (Bruker, Courtaboeuf, France) operated at 50 kV and 50 mA. The monochromatic CuK$\alpha$ radiation ($\lambda = 1.541$ Å) was focused with a 350 $\mu$m focal spot at 320 mm by a double reflection on a elliptic cross multilayer Montel mirror (Incoatec, Geesthacht, Germany). The beam was defined under vacuum by four motorized carbon-tungsten slits (JJ-Xray, Roskilde, Denmark) positioned in front of the mirror (500 $\mu$m). Four additional guard slits (600 $\mu$m) were placed at the focal point with a 220 mm slit separation. The flux after the output mica windows was $3 \times 10^8$ photons/s. A 2-mm diameter circular lead beam stop was placed in air at 150 mm after the sample, and the detector was positioned at 360 mm. The x-ray patterns were therefore recorded for a range of reciprocal spacing $q = 4\pi \sin\theta/\lambda$ (with $\theta$ the scattering angle) from 0.03 to 1.8 Å$^{-1}$, i.e., a range of repetitive distances $d = 2\pi/q$ from 200 Å to 3.5 Å. The samples were put in 1.2–1.3 mm glass capillaries (Glas Technik and Konstruktion, Schönewalde bei Berlin, Germany) and introduced into a homemade capillary holder accommodating 20 capillaries at controlled temperature or subject to a computer-monitored controlled temperature program.

For the Trp-Phe samples, SAXS was performed on the high brilliance ID2A beam line of the European Synchrotron Radiation Facility (ESRF, Grenoble, France) using sample-detector distances of 1.5–6.5 m depending on the experiments. The diffraction patterns were therefore recorded for reciprocal spacing $q$ (Å$^{-1}$) from 0.02 to 0.5 Å$^{-1}$, i.e., a range of repetitive distances $d = 2\pi/q$ from 310 Å and 12 Å. The samples were put in 1.2–1.3 mm glass capillaries and introduced into the homemade holder. The x-ray patterns were detected and recorded via a chip charge-coupled device camera detector. All samples exhibited powder diffraction and the scattering intensities as a function of the radial wave vector, $q = 4\pi \sin\theta/\lambda$ was determined by circular integration (43).

## Freeze-fracture electron microscopy and negative staining

For freeze-fracture electron microscopy, samples were prepared in a solution containing 30% glycerol. As a preliminary, SAXS patterns were recorded for the peptide solutions in the absence and presence of glycerol; all showed that the molecular and supramolecular packing of the peptide was not affected by the glycerol. The only difference observed in some cases was a shift toward higher concentration in the critical concentration of self-assembly. Droplets of samples were deposited on copper holders for double replica and frozen in LN2-cooled cryofreeze (L4194, Agar scientific, Stansted, UK). Freeze-fracturing of the double replica sandwiches was done in a Balzers BAF 300 freeze-fracture apparatus (BAL-TEC, Balzers, Liechtenstein) under $10^{-7}$ Torr vacuum, and a platinum replica of the fracture face was shadowed on fractured samples at an incidence of 45° followed by a carbon replica at 90°. Metallic replicas were floated on water and collected on copper electron microscope (EM) grids for observation under the electron microscope.

For the DTrp-DPhe derivative, the freeze-fracture was performed in the absence of glycerol. Drops of DTrp-DPhe solution were sandwiched between two copper platelets using a 400 mesh gold grid as spacer. The samples were then frozen at −180°C by rapid immersion in liquid propane and stored at −196°C in liquid nitrogen until subsequent use. Frozen samples were fractured at −150°C and $2 \times 10^{-7}$ mbar in a Balzers BAF 300 freeze-fracture apparatus. Freeze-etching was carried out by switching the sample temperature from −150°C to −100°C and maintaining the pressure at $10^{-7}$ mbar for 2 min to sublimate the surface layer of ice. Metal replicas of the exposed surfaces were obtained by evaporating 2 nm of platinum with an electron gun at an angle of 45° and 20 nm of carbon with an electron gun at an angle of 90°.

For negative staining, samples were prepared in water and deposited directly on formvar-coated nickel EM grids. After 1 min, the grids were blotted on filter work and dried. Then, samples were negatively stained with a drop of 2% uranyl acetate in water, blotted, and dried on filter work again.

EM grids (from freeze-fracture or negative staining) were observed either in a Philips 400 (FEI company, Eindhoven, The Netherlands) transmission electron microscope and photographed on Kodak SO-163 negative films (Kodak, Rochester, NY) or were examined with a JEOL 1010 transmission electron microscope (JEOL, Tokyo, Japan) at 80 kV.

## Fourier transform infrared spectroscopy

Attenuated total reflectance (ATR) Fourier transform infrared spectroscopy (FTIR) spectra were measured at 4 cm$^{-1}$ resolution with a Bruker IFS 66 spectrophotometer equipped with a 45° n ZnSe ATR attachment. The spectra shown resulted from the average of 50 scans. Spectra were corrected for the linear dependence on the wavelength of the absorption measured by ATR. The water signal was removed by subtraction of a pure water spectrum recorded the day of the experiment. Analysis of the lanreotide conformation was performed by decomposition of the absorption spectra, either as a sum of Gaussian components (44) or as a sum of spectra assigned to different structures (45).

## Fourier transform and Raman spectroscopy

Fourier transform (FT)-Raman spectra were recorded at 4 cm$^{-1}$ resolution using a Bruker IFS 66 interferometer coupled to a Bruker FRA 106 Raman module equipped with a continuous neodymium-doped yttrium aluminum garnet laser providing excitation at 1064 nm, as described in Mattioli et al. (43). All spectra were recorded at room temperature with backscattering geometry from concentrated samples (>10% w/w of lanreotide acetate) held in standard aluminum cups. The spectra resulted from 100 to 1000 coadded interferograms depending on the sample signal.

# RESULTS

## Conformational mutants: Cys-Ala, Lan-$\beta$-M, and Lys-DLys

Samples were prepared by mixing the derivatives up to 10% (w/w) with deionized water. Macroscopically, the three peptides form gels from concentrations around 2–3% (w/w). These gels all show birefringence under polarized light, indicating the formation of supramolecular architectures (data not shown). However, developable surfaces could be detected in none of these gels, as previously observed for lanreotide gels. This indicates that the gels formed by the derivatives contain more rigid structures than the lanreotide nanotubes. At concentrations above 10% (w/w), the lysine derivative peptide becomes partly insoluble and precipitates.

The peptide backbone conformation and hydrogen-bonding patterns were probed by FTIR (focusing on the amide I band). The disulfide bridge conformation was probed by

FT-Raman spectroscopy (Fig. 2). The FT-Raman spectra recorded for solutions of Lan-$\beta$-M and Cys-Ala derivatives (Fig. 2 $a$) show the disappearance of the vibrational mode at 509 cm$^{-1}$ when compared with the spectrum of lanreotide. The S-S bond stretching vibration depends on the conformation of the C-S-S-C group (46). In particular it can exhibit three different vibration wave numbers, i.e., 509, 523, and 540 cm$^{-1}$, which have been respectively assigned to $g$-$g$-$g$, $t$-$g$-$g$, and $g$-$t$-$g$ conformations. The strong vibration at 520 cm$^{-1}$ recorded on both the Lan-$\beta$-M and Cys-Ala spectra (Fig. 2 $a$, $traces~4$ and $6$) and on the Lys-DLys spectrum (Fig. 2 $c$) can be attributed to a naphthalene vibrational mode, as previously done for the lanreotide spectra (33). Although the Raman spectra of pure naphthalene, either solid or dissolved in tetrahydrofuran (THF), exhibit a slightly shifted mode, i.e., 515 and 511 cm$^{-1}$, respectively (Fig. 2 $a$, $traces~1$ and $2$), the attribution of this vibration to the naphthyl group is further supported by the spectrum obtained for a derivative lacking the naphthyl group (see $trace~3$, see Fig. 7 $a$). The shift of this vibration when compared with pure naphthalene is due to the covalent bond between the naphthyl cycle and the $\beta$-carbon atom of the naphthylalanine residue (data not shown). On the other hand, the vibration at 540 cm$^{-1}$ disappears for peptides lacking the tryptophan residue (see Fig. 7 $a$, $trace~1$). The 509 cm$^{-1}$ vibration can be attributed to a $g$-$g$-$g$ conformation of the disulfide bridge. On both spectra of Lan-$\beta$-M and Cys-Ala derivatives, the loss of this sharp vibration indicates the loss of the disulfide bond. The asymmetric aspect of the naphthyl vibration band of the Lan-$\beta$-M sample is due to the presence of $\beta$-mercaptoethanol, as shown by its corresponding FT-Raman spectra ($trace~3$, Fig. 2).

The FTIR spectra recorded for lanreotide solutions before and after reduction of the disulfide bridge are plotted in Fig. 2 $b$ ($traces~1$, $2$, $1'$, and $2'$). Upon reduction by $\beta$-mercaptoethanol, the absorptions characteristic of the backbone carbonyl groups involved in H-bonds in turn and in random conformation (absorptions at 1660 and 1640 cm$^{-1}$, respectively) almost completely disappear (Fig. 2 $c$, $traces~1'$ and $2'$). Moreover, for Lan-$\beta$-M as for Cys-Ala (Fig. 2 $b$, $trace~3$) the resulting amide I vibration absorption spectra exclusively show two maxima at 1625 and 1685 cm$^{-1}$. The presence and position of these two maxima have been described as characteristic of H-bonds in an antiparallel $\beta$-sheet conformation (47,48). The peptide FTIR global spectra are composed by the superposition of the spectra of the nonassembled peptide and of the assembled one, the contribution of the nonassembled one decreasing with concentration. To access the number of backbone carbonyls involved in such an antiparallel $\beta$-sheet network, we decomposed the FTIR spectra obtained for the highest peptide concentration into individual components (Fig. 2 and Table1). From this decomposition, the area of the two peaks at 1625 and 1685 cm$^{-1}$ represent between 82% and 87% of the total area of the amide I bands, which gives, when compared with the total number of backbone carbonyls, $\sim$7 backbone carbonyls involved in the antiparallel $\beta$-sheet network for both Cys-Ala and Lan-$\beta$-M derivatives. Taking the Raman and FTIR observations together, we can conclude that both Lan-$\beta$-M and the Cys-Ala derivative adopt a linear conformation. We also can deduce that the extended $\beta$-sheet network is formed between the linear peptides packed head-to-tail within the assemblies.
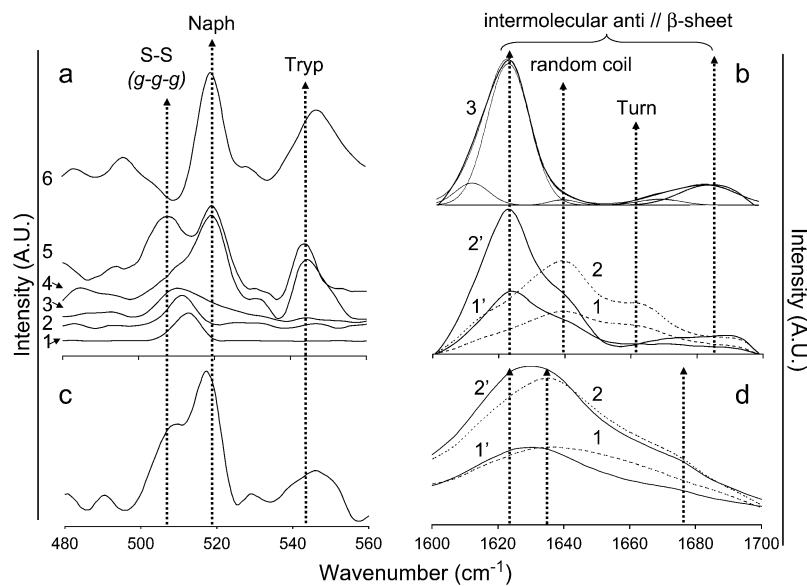


FIGURE 2   FT-Raman ($a$ and $c$) and ATR-FTIR ($b$ and $d$) spectra. ($a$) FT-Raman spectra ($\lambda$ = 1064 nm) of naphthalene powder ($trace~1$), naphthalene in THF ($trace~2$), $\beta$-mercaptoethanol ($\beta$-M) 1 M ($trace~3$), Lan-$\beta$-M 20% w/w in water ($trace~4$), lanreotide acetate 20% w/w in water ($trace~5$), and Cys-Ala acetate 15% w/w in water ($trace~6$). Dashed arrows indicate the position of the vibrations of disulfide bridge in a $g$-$g$-$g$ conformation (505 cm$^{-1}$), the naphthalene group in the peptide (520 cm$^{-1}$), and tryptophan (545–550 cm$^{-1}$). ($b$) ATR-FTIR spectra of the amide I band of lanreotide acetate 5% and 10% w/w in water ($traces~1$ and $2$, respectively) and of Lan-$\beta$-M acetate 5% and 10% w/w in water ($traces~1'$ and $2'$, respectively). ATR-FTIR spectra of Cys-Ala acetate 10% w/w in water ($trace~3$) together with the decomposition into individual components ($thin~line~peaks$ under the $spectrum$; see Table 2 for more details). Arrows indicate the position of the absorption peaks associated with the carbonyl involved in H-bonds in intermolecular $\beta$-sheet (1625 and 1685 cm$^{-1}$), random coil (1640 cm$^{-1}$), and turn (1660 cm$^{-1}$) conformations. ($c$) FT-Raman spectra ($\lambda$ = 1064 nm) of Lys-DLys acetate 15% w/w in water. For arrow definitions, see legend panel $a$. ($d$) ATR-FTIR spectra of Lys-DLys acetate 5% w/w ($traces~1$ and $1'$) and 10% w/w ($traces~2$ and $2'$) in water. The spectra were recorded either just after the dilution of the peptide in water ($traces~1$ and $2$) or 24 h after the dilution ($1'$ and $2'$).

**TABLE 1   Estimation of the number of backbone carbonyls involved in H-bond in antiparallel $\beta$-sheet conformation**

| Derivative | [Pep] w/w | Number of peaks | % Area at 1625 cm$^{-1}$ | % Area at 1685 cm$^{-1}$ | Total % area | Estimated number of carbonyls | $r^2$ |
|---|---|---|---|---|---|---|---|
| Cys-Ala | 10% | 5 | 73 | 14 | 87 | 7 | 0.998 |
| Lan-$\beta$-M | 10% | 4 | 73 | 9 | 82 | 7 | 0.997 |

This estimation was done on the spectra recorded for the highest concentration of peptide to reduce the contribution of the unstructured spectra arising from nonassembled peptides. The decomposition was performed using simple Gaussian curves (see Fig. 2).

Like lanreotide, the S-S bond of the Lys-DLys derivative can be detected in the FT-Raman spectrum (Fig. 2 *c*) by a well-defined stretching vibration band at 509 cm$^{-1}$, characteristic of a *g-g-g* conformation. The FTIR time-dependent spectra of the Lys-DLys amide I vibration (Fig. 2 *d*) recorded after dissolution of the peptide in water changed from a broad to a more structured spectrum. This indicates that the peptide backbone undergoes slow conformational changes that are probably related to slow kinetics of self-assembly. The FTIR spectrum recorded 24 h after mixing consists of a combination of $\beta$-sheet and random and turn conformations with an overall broader shape than the lanreotide spectrum (Fig. 2 *b*).

Negative staining and/or freeze-fracture electron micrographs of Lan-$\beta$-M, Cys-Ala, and Lys-DLys samples are shown in Figs. 3–5, respectively. Reduction (Lan-$\beta$-M, Fig. 3) or deletion (Cys-Ala, Fig. 4) of the disulfide bridge leads to the formation of tubular structures that are wider (diameter range: 100–200 nm) and shorter (lengths <1 $\mu$m) than the lanreotide nanotubes. On the electron micrographs of Lan-$\beta$-M, twisted ribbons coexist with wide nanotubes (Fig. 3). As the twisted ribbons have diameters similar to the tubes, it
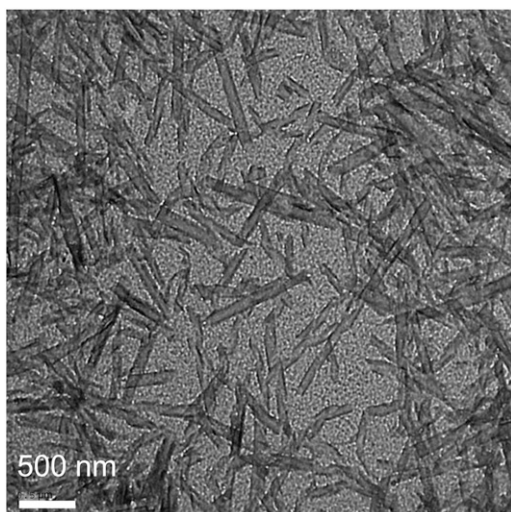


FIGURE 3   Electron micrographs obtained from negatively stained samples of Lan-$\beta$-M (5% w/w) show nanotubes shorter (<1 $\mu$m) and wider (100–200 nm) than lanreotide nanotubes.

can be assumed that they are structural intermediates of the final tubes. For the Cys-Ala derivative, such twisted ribbon intermediates were not visualized. The freeze-fracture pictures of the Cys-Ala derivative show sections of uni- or multilayered tubes (Fig. 4, *a* and *b*). Diameter analysis shows a high polydispersity for both the Cys-Ala and the Lan-$\beta$-M structures. However, the average diameter of the Lan-$\beta$-M tubes or ribbons is smaller (100 nm) than that of the Cys-Ala tubes (200 nm).

The Lys-DLys derivative forms typical amyloid-like fibers (Fig. 5, *a* and *b*) with a thickness ranging from 7 to 13 nm (Fig. 5 *c*) and with shorter lengths (up to 1 $\mu$m) than the lanreotide nanotubes. From these electron micrographs, we cannot distinguish between ribbon-like fibers and small hollow tubes. The pictures in Fig. 5, *a* and *b*, of negatively stained 10% Lys-DLys solutions were taken just after the preparation of the solution and after a few days of equilibration, respectively. They show the slow self-assembly process as seen in the time-dependent changes of the FTIR spectra.

Fig. 6 shows the WAXS patterns obtained for Lan-$\beta$-M (Fig. 6 *a*) and the Cys-Ala (Fig. 6 *b*) and Lys-DLys (Fig. 6 *c*) derivatives. In Fig. 6 *a*, the WAXS patterns obtained for increasing concentrations of Lan-$\beta$-M show the same scattering peaks. Moreover, the WAXS patterns for both Lan-$\beta$-M and Cys-Ala derivatives show similar Bragg reflections (Fig. 3). This indicates that the two peptides adopt the same molecular packing within the corresponding architectures. Considering the large nanotubes or curved lamellae formed by Lan-$\beta$-M and Cys-Ala, we can gather that the WAXS patterns reveal the molecular packing of the two-dimensional crystal that forms the walls of the assemblies. The unit cell determined from the scattering peaks is a rectangular cell with the following parameters: $a = 16.21 \pm 0.04$ Å and $b = 9.64 \pm 0.02$ Å for Lan-$\beta$-M and $a = 16.11 \pm 0.01$ Å and $b = 9.55 \pm 0.03$ Å for Cys-Ala with $\alpha = 90°$ for both peptides (see Table 2). The distance of 9.55–9.64 Å is characteristic of the repetitive distance of an antiparallel $\beta$-sheet (49), which is in full agreement with the information deduced from the FTIR spectra. We can thus conclude that the wall of the observed curved lamellae/nanotubes is built from filaments formed by head-to-tail and completely interdigitated peptides linked by an antiparallel $\beta$-sheet network in the ''b'' direction and from the lateral packing of these $\beta$-sheet filaments in the ''a'' direction. Table 3 shows a scheme of this proposed molecular packing of Cys-Ala and Lan-$\beta$-M.

The x-ray patterns recorded for the Lys-DLys derivative at different concentrations are less detailed than those obtained for the two previous derivatives (Fig. 6 *c*), although the characteristic Bragg reflections at 0.36 and 1.3 Å$^{-1}$ are also detected. Instead of scattering peaks, regular and soft oscillations are visible on the patterns that can be fitted with a cosine function with a periodicity of 0.13 Å$^{-1}$ (45 Å). Such oscillations, previously observed in soap films (50), were attributed to pair interactions between high electron density planes. In our case, they may be due to either individual layers with rich
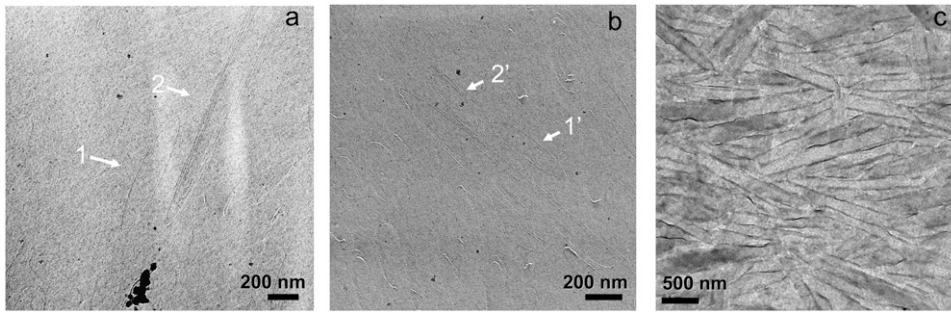
FIGURE 4 Electron micrographs obtained either from freeze-fractured (*a* and *b*) or negatively stained (*c*) samples of Cys-Ala (5% w/w in water). In *a* and *b*, the arrows indicate either unilamellar (*1* and *1'*) or multilamellar (*2* and *2'*) nanotubes

electron edges or the stacking of two quasiidentical layers, which we show as possible molecular packing in Table 3. Currently, we cannot favor one of these two solutions without x-ray fiber patterns of well-oriented samples. Moreover, none of the existing models proposed for amyloid fiber organization—including, the nanotube model proposed by Inouye et al. (40)—fitted our data. At this time, we can say only that similar x-ray patterns were reported for $\beta$-amyloid fibers (51) and that this is in agreement with the electron microscopy observations.

## Aromatic mutants: DNal-DPhe, Tyr-Phe, and DTrp-D-Phe

For these three derivatives, the FT-Raman spectra exhibit the same vibration mode around 505–509 cm$^{-1}$, which indicates that the disulfide bridge adopts a similar *g-g-g* conformation to the one adopted in lanreotide. One can also observe the disappearance of the naphthyl vibration for the DNal-DPhe derivative and of the tryptophan vibration for the DTrp-DPhe derivative due to the selective replacement of these side chains.

The FTIR spectra of the DNal-DPhe and Tyr-Phe derivatives exhibit broad and unresolved FTIR amide I vibrations (Fig. 7 *b*, *traces 4–8*) in the concentration range 5–20% (w/w). Of these two derivatives, only the Tyr-Phe derivative at 20% (w/w) exhibits slightly more structured amide I vibrations (Fig. 7, *trace 6*).

In the case of the DTrp-DPhe derivative, the FTIR amide I spectra for three different concentrations (Fig. 7 *b*, *traces 1–3*) are very similar to the lanreotide spectra. They exhibit the four sharp FTIR absorptions at 1618, 1638, 1661, and

1690 cm$^{-1}$ that are characteristic of the $\beta$-hairpin conformation and of the intermolecular antiparallel $\beta$-sheet stacking of lanreotide within the nanotubes (33).

Up to concentrations of 15% (w/w), the DNal-DPhe and the Tyr-Phe derivatives are soluble in water as clear solutions (isotropic, optical microscopy), and no gels are formed. However, in this concentration range SAXS patterns show a broad diffuse scattering around 0.15Å$^{-1}$, indicating the formation of aggregates in solution (data not shown). For DNal-DPhe, the maximum of the diffuse scattering shifts toward higher angles with increasing peptide concentration. This indicates a decrease in either the characteristic aggregate size or the interacting distance between the aggregates detected by SAXS (from 0.1 to 0.16 Å$^{-1}$ going from 5% to 30%, corresponding to a shift from 60 to 40 Å). At the concentration of 10% (w/w) the Tyr-Phe derivative shows a broad scattering peak around 0.09 Å$^{-1}$ (corresponding to a distance of 70 Å). Such a broad, diffuse scattering has been observed for lanreotide at low concentration (concentration below the critical concentration at which the nanotubes are formed) and/ or at high concentration and high temperature (for temperatures at which the nanotubes dissolved), indicating the presence of aggregates in solution (33), which are probably intermediates of the assemblies that have not yet been precisely characterized. The observation of these broad, diffuse scatterings may indicate that these derivatives form preaggregates, but since their solubility is much higher than that of lanreotide they do not, in the concentration range studied here, undergo self-assembly.

As previously observed, the SAXS patterns obtained for the DTrp-DPhe derivative from 5% to 20% (w/w) show
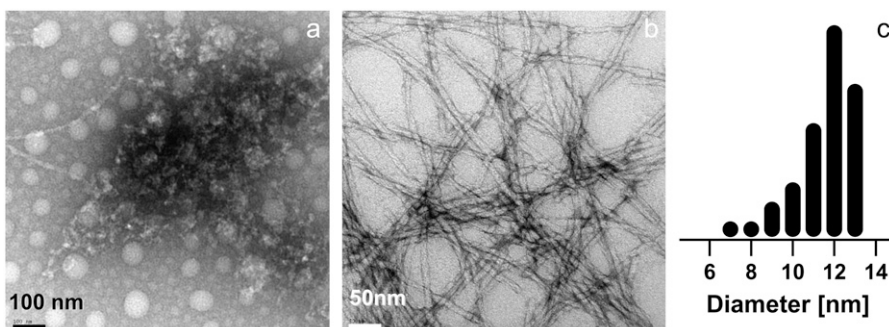


FIGURE 5 Electron micrographs obtained from negatively stained (*a* and *b*) samples of Lys-DLys (10% w/w in water, acetate) and size distribution of the width of the fibers observed (*c*). The micrographs were taken either just after the preparation of the sample (*a*) or after 1 week (*b*), showing slow fiber growth. The size distributions were plotted from ~200 measurements, indicating an average fiber width of 12 nm.
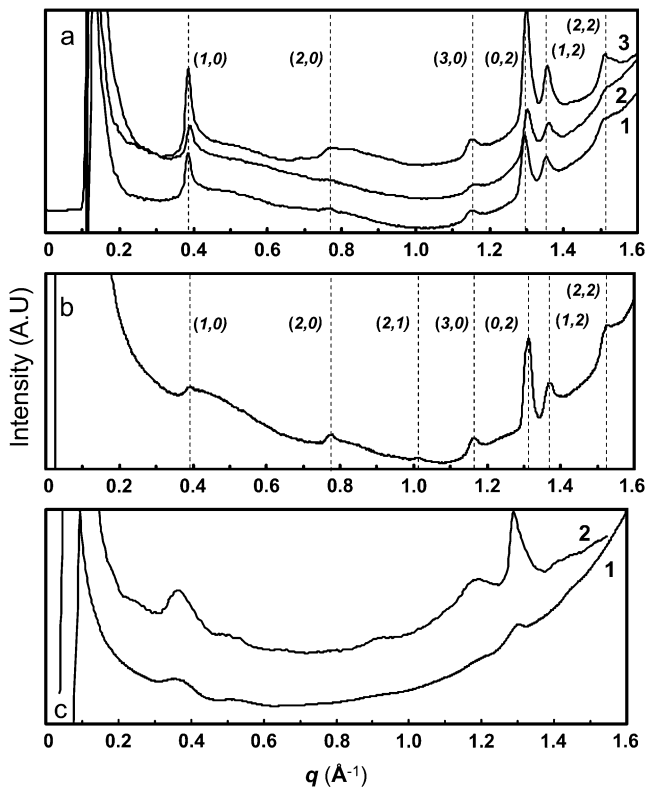
FIGURE 6   WAXS patterns of (*a*) Lanreotide-β-M, (*b*) Cys-Ala, and (*c*) Lys-DLys derivatives. (*a*) WAXS patterns of [Lan-β-M acetate] = 9%, 18%, and 30% w/w (*traces 1, 2*, and *3*, respectively). The position (*dashed lines*) and the indexing of the Bragg peaks are indicated on the graph. The indexing is detailed in Table 1. (*b*) WAXS patterns of Cys-Ala acetate 10% w/w in water. The position (*dashed lines*) and the indexing of the Bragg peaks are indicated on the graph. The indexing is detailed in Table 1. (*c*) WAXS patterns of Lys-DLys acetate 10% w/w in water.

**TABLE 2  Peak indexations of Lan-β-M and Cys-Ala derivative deduced from the x-ray patterns (Fig. 6)**

| Lan-β-M | | | | Cys-Ala | | |
|---|---|---|---|---|---|---|
| $q$ exp ($\mathring{A}^{-1}$) | $q$ theo ($\mathring{A}^{-1}$) | $d$ theo ($\mathring{A}$) | (h,k) | $q$ exp ($\mathring{A}^{-1}$) | $q$ theo ($\mathring{A}^{-1}$) | $d$ theo ($\mathring{A}$) |
| 0.39 | 0.39 | 16,26 | (1,0) | 0.40 | 0.39 | 16.09 |
| 0.77 | 0.77 | 8,13 | (2,0) | 0.78 | 0.78 | 8.05 |
| – | – | – | (2,1) | 1.02 | 1.02 | 6.15 |
| 1.16 | 1.16 | 5,42 | (3,0) | 1.17 | 1.17 | 5.36 |
| 1.30 | 1.30 | 4,83 | (0,2) | 1.31 | 1.32 | 4.76 |
| 1.36 | 1.36 | 4,63 | (1,2) | 1.38 | 1.38 | 4.57 |
| 1.52 | 1.51 | 4,15 | (2,2) | 1.54 | 1.53 | 4.10 |

The indexation was done with a rectangular lattice. The cell parameters, *a* and *b*, were found to be $a = 16.208 \pm 0.036$ Å and $b = 9.642 \pm 0.019$ Å for the Lan-β-M and $a = 16.107 \pm 0.0141$ Å and $b = 9.552 \pm 0.027$ Å for Cys-Ala. In the table, the experiment reciprocal spacings (*q* exp) are compared with those generated with the rectangular lattices (*q* theo), showing excellent agreement. The theoretical repetitive distances (*d* theo) were calculated using $d$ theo $= 2\pi/q$ theo.

values are (26, 13) for lanreotide and (18,11) for Trp-Phe derivative (34).

Freeze-fracture electron micrographs of the DNal-DPhe derivative show the formation of small ''micelle''-like aggregates of ~10 nm (Fig. 9), in agreement with the broad scattering peak in the SAXS data. Moreover, such ''micelle-like'' aggregates are very often seen as intermediates in the formation of amyloid fibers (52–54). For the tyrosine derivative, no aggregate is observed using the freeze-fracture technique. Then, if some aggregates exist, either their size is below the resolution of the technique (~3–4 nm) or they are not fractured during the preparation process.

The freeze-fracture electron micrographs of the DTrp-DPhe derivative show longitudinal fractures of nanotubes (Fig. 10). These micrographs show that the nanotubes are

regular oscillations, as for lanreotide (34). The fit of the patterns by a zero order Bessel function indicates that the DTrp-DPhe derivative in solution forms rigorously monodisperse nanotubes 16 nm in diameter. This diameter is independent of the peptide concentration in the range 5–20% (w/w). For concentrations higher than 20% (w/w), the monodispersity is lost, as shown by the disappearance of the oscillations. The SAXS patterns look like those obtained for lanreotide when embedded nanotubes are formed (33). Like lanreotide, the DTrp-DPhe nanotubes are packed in a disordered hexagonal lattice, as shown by the corresponding broad Bragg reflections in Fig. 8 *b*. Temperature increase induces a decrease in the hexagonal parameter (from 260 Å at 10°C to 235 Å at 70°C) without any change in nanotube diameter (Fig. 8 *c*). This behavior is similar to that of lanreotide solutions. Moreover, all the structural and molecular data indicate that the molecular and supramolecular packing of the Trp-Phe derivative is identical to that of lanreotide, as indicated in Table 3. The only differences between the two molecular packings within the nanotubes are the number of filaments *n* and the unit cell longitudinal shift along these filament for a complete round of the nanotube. The (*n*, *m*)

**TABLE 3  Self-assembling lanreotide derivatives: self-assembly morphologies and proposed molecular packing**



| Derivative | Morphologies | Possible molecular packing | Molecular conformation |
|---|---|---|---|
| Lys-DLys | Amyloid fibres | * Anti// H-bond, Peptide backbone | Cyclic / Backbone perpendicular to the plane |
| DTrp-DPhe | nanotubes | Anti// H-bond, Specific π-π stacking, peptide backbone | β-Hairpin / Backbone in plane |
| Cys-Ala & Lan β-M | nanotubes | Anti// H-bond, Peptide backbone | Linear / Backbone perpendicular to the plane |

*Part of the figure has been taken from Aggeli et al. (38) ''copyright (© 2001) National Academy of Sciences, USA''.
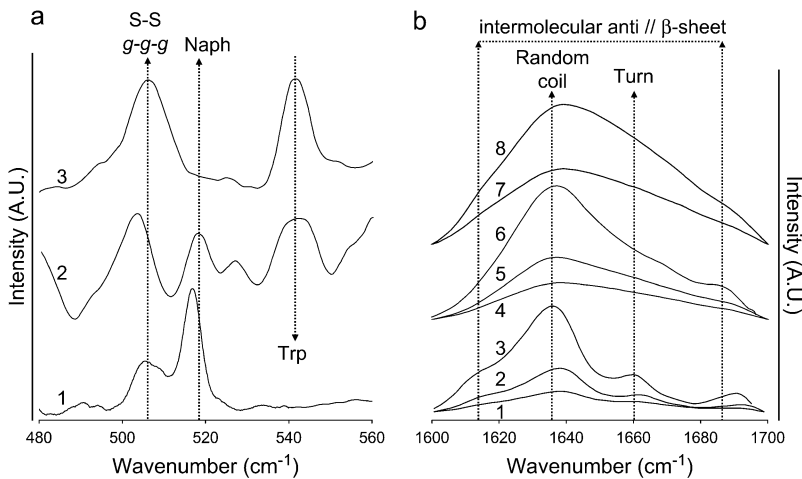
FIGURE 7   FT-Raman spectra (*a*) and ATR-FTIR spectra (*b*). (*a*) FT-Raman spectra of DTrp-DPhe acetate 10% w/w in water (*trace 1*), Tyr-Phe acetate 15% w/w in water (*trace 2*), and DNal-DPhe acetate 10% w/w in water (*trace 3*). Arrows indicate the position of scattering mode of the disulfide bridge in a *g-g-g* conformation (505 cm$^{-1}$) of naphthalene in the peptides (520 cm$^{-1}$) and of tryptophan (545–550 cm$^{-1}$). (*b*) ATR-FTIR spectra of the amide I vibrations of DTrp-DPhe acetate 5%, 10%, and 15% (*traces 1, 2,* and *3,* respectively) w/w in water of Tyr-Phe acetate 5%, 10%, and 20% (*traces 4, 5,* and *6,* respectively) w/w in water and of DNal-DPhe acetate 5% and 10% (traces 7 and 8, respectively) w/w in water. Arrows indicate the positions of the absorption peaks associated with the carbonyl involved in H-bonds in intermolecular $\beta$-sheet (1625 and 1685 cm$^{-1}$), random coil (1640 cm$^{-1}$), and turn (1660 cm$^{-1}$) conformations.

tightly packed parallel to each other, as expected from the hexagonal organization of the nanotubes revealed by the SAXS patterns.

## DISCUSSION

Lanreotide, a small peptide of eight amino acids, possesses all the molecular parameters driving its self-assembly in the presence of water. The self-assembly process of lanreotide is controlled by the balance between two opposite forces, i.e., hydrophobic effects, which result in water in an ''attraction'' between peptides and repulsive electrostatic interactions. Furthermore, the molecular parameters drive the molecular packing; and to obtain detailed information on these molecular parameters we adopted a site-directed mutational approach.

We chose either to mutate residues that modify the conformation of the molecule or to successively substitute the three aromatic residues by a phenylalanine. Besides this precise purpose, the mutations we chose to apply to lanreotide are also related to more general questions. The influence of peptide conformation on molecular packing in self-assembly is, for example, relevant to amyloid peptides but also to bio-nanomaterials. In addition, $\pi$-stacking has been postulated as an important type of interaction driving amyloid fibril growth (3,27,55). Lanreotide and its derivatives are powerful tools in elucidating the involvement of $\pi-\pi$ interactions and the peptide backbone conformation in peptide self-assembling processes. Moreover, understanding these types of interactions can help to design new molecules capable of forming desired supramolecular architectures.
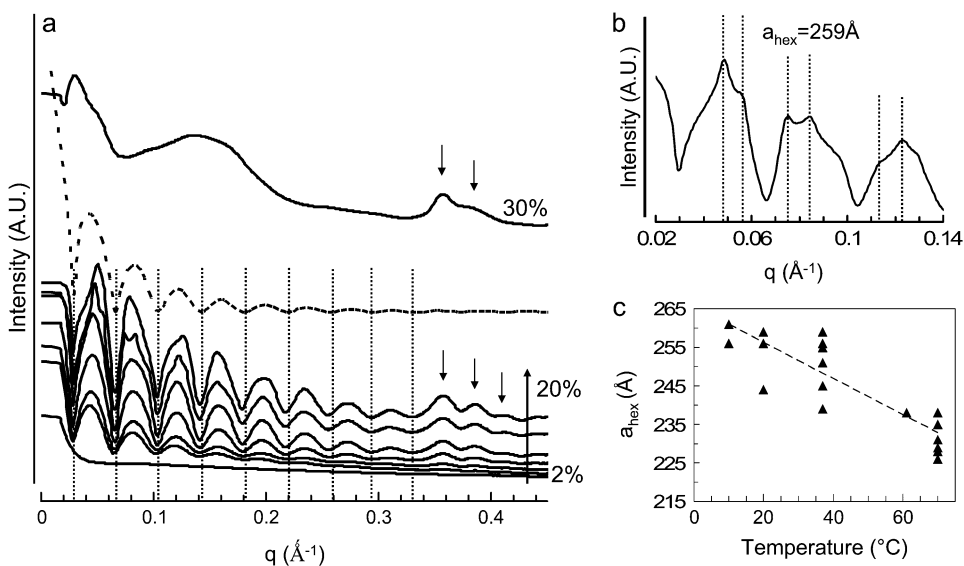


FIGURE 8   SAXS patterns of DTrp-DPhe samples obtained with a sample to detector distance of 1.5 m (*a*) and of 6.5 m very small angle x-ray scattering (*b*) on ID2 beam line (ESRF, Grenoble) and change in the hexagonal parameter with temperature (*c*). (*a*) SAXS patterns as a function of DTrp-DPhe acetate concentration (sample to detector distance of 1.5 m). The seven lower patterns were obtained for 2%, 4%, 5%, 8%, 10%, 15%, and 20% (w/w) of peptide acetate in water. The dashed curve is a $J_0$ Bessel function calculated for a radius of 82 nm. The dotted lines i), underline the minima of the Bessel function that fit with the experimental ones, and ii), show that these minima are independent on peptide concentration. The upper curve was obtained for 30% (w/w) of peptide acetate in solution. The arrows underline the diffuse scattering peaks induced by the antiparallel $\beta$-sheet network. (*b*) SAXS patterns obtained for 14% (w/w) of peptide acetate in water at 20°C (sample to detector distance of 6.5 m). The dashed lines are in the theoretical position of the Bragg peaks expected for a hexagonal lattice of 259 Å to underline that the experimental peak positions are in agreement with the theoretical ones. (*c*) Change in the hexagonal lattice parameter with temperature. These data were obtained for 8%, 10%, 14%, and 20% (w/w) peptide acetate in solution during the heating and cooling process.
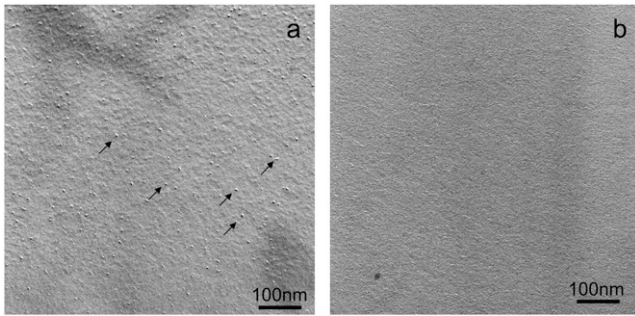
FIGURE 9 Electron micrographs obtained from freeze-fractured solutions of DNal-DPhe acetate 10% w/w in water/glycerol (*a*) and Tyr-Phe acetate 10% w/w in water/glycerol (*b*). Arrows in *a* underline some of the "micellar"-type aggregates. No aggregates were observed in *b*.

Fig. 11 summarizes the results obtained on the behavior of the different peptides in water, in terms of assembly, morphology, and molecular conformation. We schematized the possible molecular packing that matches our experimental data. As a general survey, the modifications designed to affect the conformation of lanreotide, i.e., Lan-β-M and Cys-Ala, on the one hand, and Lys-DLys, on the other, allowed the peptide to retain its capacity to form supramolecular architectures involving β-sheet networks. However, they modified the morphology and the molecular packing of the assemblies more deeply than lanreotide did. Peptide conformation thus plays a role in molecular packing within the self-assemblies but does not affect the self-assembling propensity of the peptides. On the contrary, slight mutations in the aromatic residues either considerably decrease the self-assembly capacity of the peptide and its propensity to develop extended β-sheet structures (DNal-DPhe and Tyr-Phe) or modify only the final diameter
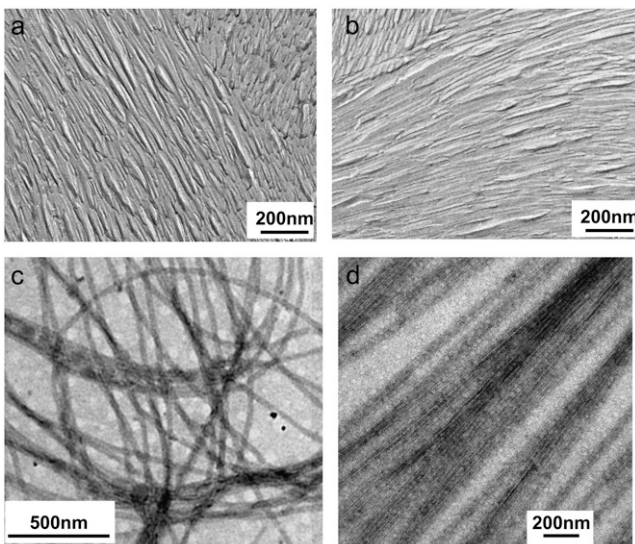


FIGURE 10 Electron micrographs of replicas of freeze-fractured and etched solution of DTrp-DPhe acetate 10% w/w (*a* and *b*) and of negatively stained solution of DTrp-DPhe acetate 8% w/w in water (*c* and *d*).

of the nanotubes while keeping the molecular packing identical to that of lanreotide (DTrp-DPhe) (34). This show that the three aromatic side chains do not have equivalent roles in the self-assembly process: the naphthalene and tyrosine side chains (in the initial lanreotide sequence) play the role of highly specific molecular "glue" whereas the tryptophan side chain is involved in the lateral filament stacking.

## Which molecular parameters drive self-assembly?

The idea that $\pi-\pi$ stacking is one of the driving forces of peptide-protein fiber formation emerged a few years ago. E. Gazit (56) reviewed studies on peptides extracted from the sequence of amyloid-forming proteins that kept the self-assembling properties of the entire protein. All these amino acid sequences contained a high number of aromatic residues. Knowing that aromatic residues are among the less frequently occurring amino acids, this observation is not trivial. Moreover, directed mutations systematically replacing these amino acids by Ala showed that all but the aromatic amino acids can be replaced by Ala without changing the propensity for self-assembly. Indeed, the replacement of the aromatic residues by Ala completely inhibited this capacity. It was further suggested that $\pi-\pi$ stacking provides an energetic contribution as well as order and directionality to the self-assembly of amyloid structures.

The lanreotide sequence contains three aromatic amino acids in a total of eight. Besides these hydrophobic aromatic residues, it has two positive charges, which explain the high solubility of the peptide since nanotube assembly occurs at concentrations higher than 30 mM. Among the residues substituted in this study, we successively mutated the three aromatic residues into phenylalanine. We chose to mutate these aromatic side chains to another aromatic one and not, as Gazit did (56), to a simple Ala for two major reasons: i), we already knew from the segregation of the aromatic side chains in the self-assemblies that these residues played a major role involving $\pi-\pi$ stacking, and ii), we wanted to know if these aromatic residues had some specific features. The minimal mutations DNal-DPhe and Tyr-Phe strongly affect the solubility of the peptide. Indeed, these two mutants do not form nanotubes or any other nanoscale self-assemblies based on extended intermolecular β-sheet, at least in the concentration range studied in this work, i.e., concentrations up to 10 times the critical concentration of lanreotide (300 mM). These results indicate that these mutations together increased the solubility of the peptide and decreased its self-assembling propensity. The aromatic interactions in lanreotide nanotubes, consequently, not only are related to simple $\pi-\pi$ interactions but also involve some more specific interactions. For information, we also tested the mutation of DNal into DAla. The behavior of this peptide was comparable to that of the mutant reported in this work (data not shown). From this study, we conclude that two of the three aromatic residues in the lanreotide sequence are directly involved in the intermo-

lecular peptide-peptide interaction. These results are also in agreement with the idea developed by C. Dobson that to avoid protein fiber formation, nature has developed strategies to increase the solubility of the protein in solution (20). The presence of aromatic residues that are generally hydrophobic decreases the solubility of the peptides/proteins. Furthermore, as they can interact through $\pi-\pi$ stacking, these residues can orient the peptide-peptide interactions. From our data, we propose that aromatic-aromatic interactions drive such a self-assembly process. In the case of lanreotide, we propose that the DNal and the Tyr, due to their capacities through $\pi-\pi$ interactions to orientate the self-assembly, represent the molecular ''glue''. Moreover, our experiments show that aromaticity is not enough. In particular, the behavior of the Tyr-Phe derivative compared with that of lanreotide raises the question of the specificity of this aromatic side chain. In recent preliminary Raman experiments we showed a very unusual modification of the Tyr environment in relation to its propensity to form H-bonds within the assemblies (57). Further experiments are required and have been undertaken to fully characterize the role of Tyr in the self-assembly process. However, this new molecular information supports the idea that at least part of the specificity of Tyr in lanreotide self-assembly is related to its capacity to act as an H-bound donor and/or acceptor. Of course, this conclusion does not exclude the involvement of the electron donor/acceptor properties of the aromatic cycle in the self-assembly process of lanreotide. Altogether, these results demonstrate that lanreotide self-assembly is driven by specific aromatic-aromatic interactions.

## What is the relationship between the morphology of self-assembly and the conformation of the molecule?

The amino acids of lanreotide have a very particular spatial distribution relative to the peptide backbone. Lanreotide can be described as a cyclic peptide, with one face of the cycle being essentially hydrophilic and the other hydrophobic. Moreover, the peptide sequence induces a strict segregation of the aliphatic and aromatic lateral chains pointing to the hydrophobic face of the cycle. The conformational mutants generated in this study, besides changing the conformation of the peptide backbone, modified the distribution of the hydrophobic and hydrophilic residues relative to the face of the peptide cyclic backbone.

In terms of amino acid sequence and among the mutations considered here, the Lys-DLys mutation is the mildest. Indeed, the sequence is identical to that of lanreotide, the only change being the configuration of the Lys side chain. From NMR studies on lanreotide in organic solvents, the monomer conformation has been characterized as a $\beta$-hairpin stabilized by a disulfide bridge. Moreover, a strong interaction has been detected between the DTrp and the Lys residues (42) in the $\beta$-turn of the molecule. We have further shown in our previous work (34) that this $\beta$-hairpin conformation is stabilized

for lanreotide in nanotube assemblies. Moreover, the structure of the nanotubes strongly suggests that the Nal, Tyr, and Val amino acids point toward the hydrophobic face of the peptide, whereas the Trp and Lys together point toward the hydrophilic face. So, in the Lys-DLys mutant, the Lys pointing toward the hydrophilic face of the wild-type peptide now points toward the initially hydrophobic face of the backbone, inducing a drastic decrease in the amphiphilicity of the peptide compared with lanreotide. This modification drastically affects the molecular packing and consequently the architectures formed. Instead of the well-organized two-dimensional crystals for lanreotide in the nanotubes, the Lys-DLys derivative self-assembles in a less ordered one-dimensional amyloid-type liquid crystal. The corresponding x-ray patterns and electron micrographs are similar to those obtained for amyloids, observed either for entire prion proteins (51) or for peptides extracted from prion protein sequences (3). Unfortunately, our structural data are too poor to give the precise molecular packing of Lys-DLys within the fibers. However, we can say that they are formed by the lamination of 5–6 layers of peptide filaments, reaching a final average size of ~10–12 nm. Since the hydrophobic and hydrophilic residues of the peptide are no longer segregated on each face of the cyclic peptide, the face-to-face dimer cannot be formed. The peptide-peptide interactions, even if they are still driven by the aromatic residues, must have a topology that is different from lanreotide's. In Table 3, we propose that the Lys-DLys fibers are formed by a peptide bilayer, with the H-bond network in one direction and the aromatic-aromatic interactions in the other. The latter interactions can be either located at the C-terminal (1) and then mediated by the Naph or located in the turn (4) and then mediated by the DTrp.

The molecular packing characterized for the opened lanreotide sequence (either by mutation or by reduction of the disulfide bridge) can also be explained by a drastic change in the amphiphilicity of the molecule. In these cases, the hydrophobic and hydrophilic residues are distributed along the linear peptide backbone without any specific topology. The peptide has the same solubility as lanreotide globally, but the x-ray data do not show any systematic segregation of the aromatic residues from the aliphatic ones. These residues are not orientated with respect to the peptide backbone as they were for lanreotide. The molecular packing of the lamellar sheets observed for the Cys-Ala derivative and Lan-$\beta$-M are characterized by the lateral association of filaments, i.e., lamination of filaments. These filaments are formed by an antiparallel H-bond network between head-to-tail peptides (Table 3), and the interactions between filaments are probably mediated by aromatic interactions. Such lamination of amyloid fibrils forming helical ribbons that further close into large hollow cylinders (as we saw for the Lan-$\beta$-M) has been observed for the linear amyloid peptides A$\beta$-(16–22) (58). Interestingly, these authors proposed that the size of the final fiber depends on the extent of lamination of the fibrils and that the peptide size reduction increases the extent of lamination. In the case of

the Cys-Ala derivative, which forms large nanotubes by fibril lamination, we are indeed in the same peptide size range as that for Aβ-(16–22). Unlike amyloid peptides, the nanotubes are formed here by an interdigitated monolayer of the linear form of lanreotide and not by a bilayer of peptides.

In conclusion, we propose that amphiphilicity drives the molecular packing, which then drives the morphology, of the final architectures formed.

## How is nanotube diameter modulated?

Lanreotide nanotubes are composed of 26 laterally assembled helicoidal filaments. These filaments are formed by the stacking of dimer building blocks through two different antiparallel H-bond networks, i.e., two different protofilaments, one external and one internal to the nanotube walls (34). The contacts between the external and the internal protofilaments are not equivalent. Indeed, the difference in periphery for the external and the internal layer is $\sim 1/2(2\pi e)$ (e being the thickness of the nanotubes wall), i.e., $\sim 5.6$ nm. This means that the distance between the 26 external and internal protofilaments differ by 0.22 nm. This value represents $\sim 10\%$ of the total length of the β-hairpin peptide (2 nm). In this study, we show that the substitution of the DTrp (position 4, in the lanreotide turn) by DPhe reduces the diameter of the nanotubes from 24.4 to 16 nm without affecting the molecular packing. This particular aromatic residue is probably not involved in dimer stacking, unlike DNal (1) and Tyr (3) in the lanreotide sequence, but is likely involved in the association of the filaments that form the nanotubes. This also suggests that this particular amino acid is involved in the close contact between the protofilaments. The other very important conclusion is that the lanreotide self-assembly process is rather insensitive to specific properties of the aromatic side chain in this position, indicating essentially that $\pi-\pi$ stacking is involved in the lateral interaction between the protofilaments.

## CONCLUSIONS

The aim of this study was to gain information on the molecular parameters that lead to the remarkable self-assembly process of lanreotide in water. We demonstrate that the two aromatic residues DNal (1) and Tyr (3) drive the self-assembly process by specific aromatic/aromatic interactions that can be electron and/or H-bond donor/acceptor. Indeed, mutations of these two aromatic residues drastically decrease the peptide's propensity to self-assemble by increasing the solubility of the peptide and by decreasing the aromatic stacking strength. We also show that any mutation changing the spatial organization of the hydrophilic and hydrophobic residues, i.e., the amphipathic pattern of the molecule, modifies the molecular packing and changes the final supramolecular architecture. We characterize three different molecular packing regimes that lead to three different morphologies, i.e., i), lamellae formed by an interdigitated monolayer of peptides; ii), nanotubes formed by face-to-face dimer stacking; and iii), amyloid fibers formed by the lamination of $n$-dimensional fibrils (Table 3). These supramolecular architectures are all stabilized by aromatic interactions and antiparallel β-sheet networks. Finally, we show that the aromatic residue located in the β-turn of lanreotide is involved in the lateral packing of the filaments and therefore in fixing the final monodisperse diameter of the nanotubes. Moreover, unlike D-Nal and Tyr, no strong specificity is observed for the aromatic side chain in position 4, as only $\pi-\pi$ stacking is involved in this interaction.

The extreme sensitivity of the self-assembly processes of lanreotide to the molecular sequence of the peptide provides information that can be related to the molecular parameters driving amyloid-related self-assemblies. Finally, this work also describes some of the parameters necessary for the bottom-up design of new peptide families that self-assemble into tunable nanotubule or fibril architectures.

## REFERENCES

1. Chiti, F., M. Calamai, N. Taddei, M. Stefani, G. Ramponi, and C. Dobson. 2002. Studies of the aggregation of mutant proteins in vitro provide insights into the genetics of amyloide diseases. *Proc. Natl. Acad. Sci. USA.* 99:16419–16426.

2. Makin, O. S., and L. C. Serpell. 2005. Structures for amyloid fibrils. *FEBS J.* 272:5950–5961.

3. Makin, O. S., E. Atkins, P. Sikorski, J. Johansson, and L. C. Serpell. 2005. Molecular basis for amyloid fibril formation and stability. *Proc. Natl. Acad. Sci. USA.* 102:315–320.

4. Papanikolopoulou, K., G. Schoehn, V. Forge, V. T. Forsyth, C. Riekel, J. F. Hernandez, R. W. Ruigrok, and A. Mitraki. 2005. Amyloid fibril formation from sequences of a natural β-structured fibrous protein, the adenovirus fiber. *J. Biol. Chem.* 280:2481–2490.

5. Gao, X., and H. Matsui. 2005. Peptide-based nanotubes and their applications in bionanotechnologies. *Adv. Mater.* 17:2037–2050.

6. Kimbara, K., and A. Takuso. 2005. Toward intelligent molecular machines: directed motions of biological and artificial molecules and assemblies. *Chem. Rev.* 105:1377–1400.

7. Shimitzu, T., M. Masuda, and H. Minamikawa. 2005. Supramolecular nanotube architectures based on amphiphilic molecules. *Chem. Rev.* 105:1401–1443.

8. Hoeben, F., P. Jonkheijm, E. Meijer, and A. Schenning. 2005. About supramolecular assemblies of pi-conjugated systems. *Chem. Rev.* 105:1491–1546.

9. Rajagopal, K., and J. P. Schneider. 2004. Self-assembling peptides and proteins for nanotechnological applications. *Curr. Opin. Struct. Biol.* 14:480–486.

10. Bong, D. T., T. D. Clark, J. R. Granja, and M. R. Ghadiri. 2001. Self-assembling organic nanotubes. *Angew. Chem. Int. Ed. Engl.* 40:988–1011.

11. Bong, D. T., and M. R. Ghadiri. 2001. Self-assembling cyclic peptide cylinders as nuclei for crystal engineering. *Angew. Chem. Int. Ed. Engl.* 40:2163–2166.

12. Ghadiri, M. R., J. R. Granja, R. A. Milligan, D. E. McRee, and N. Khazanovich. 1993. Self-assembling organic nanotubes based on a cyclic peptide architecture. *Nature.* 366:324–327.

13. Zhang, S. 2003. Fabrication of novel biomaterials through molecular self-assembly. *Nat. Biotechnol.* 21:1171–1178.

14. Virshow, R. 1854. About a substance found in human brain and spinal marrow that reacts chemically as cellulose. *Virshow Archives Pathology. Anatomy & Physiology.* 6:135–138.

15. Divry, P., and M. Flokin. 1927. Les propriétés optiques des amyloides. *C.R. Soc. Biol (Paris).* 97:1808–1810.

16. Fandrich, M., M. A. Fletcher, and C. M. Dobson. 2001. Amyloid fibrils from muscle myoglobin. *Nature.* 410:165–166.

17. Jimenez, J. L., E. J. Nettleton, M. Bouchard, C. V. Robinson, C. M. Dobson, and H. R. Saibil. 2002. The protofilament structure of insulin amyloid fibrils. *Proc. Natl. Acad. Sci. USA.* 99:9196–9201.

18. Luckey, M., J. Hernandez, G. Arlaud, V. T. Forsyth, R. W. Ruigrok, and A. Mitraki. 2000. A peptide from the adenovirus fiber shaft forms amyloid-type fibrils. *FEBS Lett.* 468:23–27.

19. Reference deleted in proof.

20. Johnson, R. J., J. Christodoulou, M. Dumoulin, G. L. Caddy, M. J. Alcocer, G. J. Murtagh, J. R. Kumita, G. Larsson, C. V. Robinson, D. B. Archer, B. Luisi, and C. M. Dobson. 2005. Rationalising lysozyme amyloidosis: insights from the structure and solution dynamics of T70N lysozyme. *J. Mol. Biol.* 352:823–836.

21. Chapman, M. R., L. S. Robinson, J. S. Pinkner, R. Roth, J. Heuser, M. Hammar, S. Normark, and S. J. Hultgren. 2002. Role of *Escherichia coli* curli operons in directing amyloid fiber formation. *Science.* 295:851–855.

22. Claessen, D., R. Rink, W. de Jong, J. Siebring, P. de Vreugd, F. G. Boersma, L. Dijkhuizen, and H. A. Wosten. 2003. A novel class of secreted hydrophobic proteins is involved in aerial hyphae formation in Streptomyces coelicolor by forming amyloid-like fibrils. *Genes Dev.* 17:1714–1726.

23. Gebbink, M. F., D. Claessen, B. Bouma, L. Dijkhuizen, and H. A. Wosten. 2005. Amyloids—a functional coat for microorganisms. *Nat. Rev. Microbiol.* 3:333–341.

24. Serpell, L. C., C. C. Blake, and P. E. Fraser. 2000. Molecular structure of a fibrillar Alzheimer's A $\beta$ fragment. *Biochemistry.* 39:13269–13275.

25. Gazit, E. 2002. Mechanistic studies of the process of amyloid fibrils formation by the use of peptide fragments and analogues: implications for the design of fibrillization inhibitors. *Curr. Med. Chem.* 9:1725–1735.

26. Gazit, E. 2002. A possible role for pi-stacking in the self-assembly of amyloid fibrils. *FASEB J.* 16:77–83.

27. Tracz, S. M., A. Abedini, M. Driscoll, and D. P. Raleigh. 2004. Role of aromatic interactions in amyloid formation by peptides derived from human amylin. *Biochemistry.* 43:15901–15908.

28. Lynn, D. G., and S. C. Meredith. 2000. Review: model peptides and the physicochemical approach to $\beta$-amyloids. *J. Struct. Biol.* 130:153–173.

29. Benzinger, T. L., D. M. Gregory, T. S. Burkoth, H. Miller-Auer, D. G. Lynn, R. E. Botto, and S. C. Meredith. 1998. Propagating structure of Alzheimer's $\beta$-amyloid(10–35) is parallel $\beta$-sheet with residues in exact register. *Proc. Natl. Acad. Sci. USA.* 95:13407–13412.

30. Stromer, T., and L. C. Serpell. 2005. Structure and morphology of the Alzheimer's amyloid fibril. *Microsc. Res. Tech.* 67:210–217.

31. Sikorski, P., E. D. Atkins, and L. C. Serpell. 2003. Structure and texture of fibrous crystals formed by Alzheimer's A $\beta$(11–25) peptide fragment. *Structure.* 11:915–926.

32. Inouye, H., and D. A. Kirschner. 2006. X-Ray fiber and powder diffraction of PrP prion peptides. *Adv. Protein Chem.* 73:181–215.

33. Valery, C., F. Artzner, B. Robert, T. Gulick, G. Keller, C. Grabielle-Madelmont, M. L. Torres, R. Cherif-Cheikh, and M. Paternostre. 2004. Self-association process of a peptide in solution: from $\beta$-sheet filaments to large embedded nanotubes. *Biophys. J.* 86:2484–2501.

34. Valery, C., M. Paternostre, B. Robert, T. Gulik-Krzywicki, T. Narayanan, J. C. Dedieu, G. Keller, M. L. Torres, R. Cherif-Cheikh, P. Calvo, and F. Artzner. 2003. Biomimetic organization: octapeptide self-assembly into nanotubes of viral capsid-like dimension. *Proc. Natl. Acad. Sci. USA.* 100:10258–10262.

35. Janecka, A., M. Zubrzycka, and T. Janecki. 2001. Somatostatin analogs. *J. Pept. Res.* 58:91–107.

36. Blaurock, A. E., and A. E. Walsby. 1976. Crystalline structure of the gas vesicle wall from Anabaena flos-aquae. *J. Mol. Biol.* 105:183–199.

37. Blaurock, A. E., and A. E. Walsby. 1976. Structure of the wall of Halobacterium halobium Gas vesicles. *J. Mol. Biol.* 106:871–888.

38. Aggeli, A., I. A. Nyrkova, M. Bell, R. Harding, L. Carrick, T. C. McLeish, A. N. Semenov, and N. Boden. 2001. Hierarchical self-assembly of chiral rod-like molecules as a model for peptide $\beta$-sheet tapes, ribbons, fibrils, and fibers. *Proc. Natl. Acad. Sci. USA.* 98:11857–11862.

39. Jimenez, J. L., J. I. Guijarro, E. Orlova, J. Zurdo, C. M. Dobson, M. Sunde, and H. R. Saibil. 1999. Cryo-electron microscopy structure of an SH3 amyloid fibril and model of the molecular packing. *EMBO J.* 18:815–821.

40. Inouye, H., D. Sharma, W. J. Goux, and D. A. Kirschner. 2006. Structure of core domain of fibril-forming PHF/Tau fragments. *Biophys. J.* 90:1774–1789.

41. Verheyden, P., W. Francq, H. Pepermans, and G. Van Binst. 1990. Conformational study of a somatostatin analogue in DMSO/water by 2D NMR. *Biopolymers.* 30:855–860.

42. Van Binst, G., and D. Tourwe. 1992. Backbone modifications in somatostatin analogues: relation between conformation and activity. *Pept. Res.* 5:8–13.

43. Narayanan, T., O. Diat, and P. Bosecke. 2001. SAXS and USAXS on the high brilliance beamline at the ESRF. *Nucl. Instrum. Methods Phys. Res. A.* 467:1005–1009.

44. Byler, M., and H. Susi. 1986. Examination of the secondary structure of proteins by deconvolved FTIR spectra. *Biopolymers.* 25:469–487.

45. Venyaminov, S. Y., and N. N. Kalnin. 1990. Quantitative IR spectrophotometry of peptide compounds in water ($H_2O$) solutions. 2. Amide absorption-bands of polypeptides and fibrous proteins in $\alpha$-coil, $\beta$-coil, and random coil conformations. *Biopolymers.* 30:1259–1271.

46. Sugeta, H., A. Go, and T. Miyazawa. 1973. Vibrational spectra and molecular conformations of dialkyl disulfides. *Bull. Chem. Soc. Jpn.* 46:3407–3411.

47. Krause, E., M. Beyermann, H. Fabian, M. Dathe, S. Rothemund, and M. Bienert. 1996. Conformation of a water-soluble $\beta$-sheet model peptide—a circular dichroism and Fourier-transform infrared spectroscopic study of double D-amino acid replacements. *Int. J. Pept. Protein Res.* 48:559–568.

48. Janek, K., J. Behlke, J. Zipper, H. Fabian, Y. Georgalis, M. Beyermann, M. Bienert, and E. Krause. 1999. Water-soluble $\beta$-sheet models which self-assemble into fibrillar structures. *Biochemistry.* 38:8246–8252.

49. Fraser, R. D. B., and T. P. MacRae. 1973. Conformation in Fibrous Proteins. Academic Press, New York.

50. Etrillard, J., M. A. V. Axelos, I. Cantat, F. Artzner, A. Renault, T. Weiss, R. Delannay, and F. Boue. 2005. In situ investigations on organic foam films using neutron and synchrotron radiation. *Langmuir.* 21:2229–2234.

51. Kirschner, D. A., C. Abraham, and D. J. Selkoe. 1986. X-Ray diffraction from intraneuronal paired helical filaments and extraneuronal amyloid fibers in Alzheimer disease indicates cross-$\beta$ conformation. *Proc. Natl. Acad. Sci. USA.* 83:503–507.

52. Lomakin, A., D. S. Chung, G. B. Benedek, D. A. Kirschner, and D. B. Teplow. 1996. On the nucleation and growth of amyloid $\beta$-protein fibrils: detection of nuclei and quantitation of rate constants. *Proc. Natl. Acad. Sci. USA.* 93:1125–1129.

53. Goldsbury, C. S., S. Wirtz, S. A. Muller, S. Sunderji, P. Wicki, U. Aebi, and P. Frey. 2000. Studies on the in vitro assembly of A $\beta$ 1–40: implications for the search for A $\beta$ fibril formation inhibitors. *J. Struct. Biol.* 130:217–231.

54. Goldsbury, C., P. Frey, V. Olivieri, U. Aebi, and S. A. Muller. 2005. Multiple assembly pathways underlie amyloid-$\beta$ fibril polymorphisms. *J. Mol. Biol.* 352:282–298.

55. Zurdo, J., J. I. Guijarro, J. L. Jimenez, H. R. Saibil, and C. M. Dobson. 2001. Dependence on solution conditions of aggregation and amyloid formation by an SH3 domain. *J. Mol. Biol.* 311:325–340.

56. Gazit, E. 2005. Mechanisms of amyloid fibril self-assembly and inhibition. Model short peptides as a key research tool. *FEBS J.* 272:5971–5978.

57. Pandit, A., N. Fay, L. Bordes, C. Valery, R. Cherif-Cheikh, B. Robert, F. Artzner, and M. Paternostre. 2007. Self-assembly of the octapeptide lanreotide and lanreotide-based derivatives: the role of the aromatic residues. *J. Pept. Sci.* 11:66–75.

58. Lu, K., J. Jacob, P. Thiyagarajan, V. P. Conticello, and D. G. Lynn. 2003. Exploiting amyloid fibril lamination for nanotube self-assembly. *J. Am. Chem. Soc.* 125:6391–6393.